Research Article | Vol. 25, No. 2 | 23 Jan 2017 | OPTICS EXPRESS 1505

Optics EXPRESS

4-W, 100-kHz, few-cycle mid-infrared source with sub-100-mrad carrier-envelope phase noise

NICOLAS THIRÉ,[1,*] RAMAN MAKSIMENKA,[1] BÁLINT KISS,[2] CLÉMENT FERCHAUD,[1] PIERRE BIZOUARD,[1] ERIC CORMIER,[2] KÁROLY OSVAY,[2] AND NICOLAS FORGET[1]

[1]*Fastlite, 1900 route des Crêtes, Les Collines de Sophia, Bât. D1, 06560, Valbonne, France*
[2]*ELI-HU Non-Profit Ltd, Dugonics tér 1, 6720 Szeged, Hungary*
[*]*nicolas.thire@fastlite.com*

Abstract: We demonstrate an optical parametric chirped-pulse amplifier delivering 4-cycles (38-fs) pulses centered around 3.1 µm at 100-kHz repetition rate with an average power of 4 W and an undersampled single-shot carrier-envelope phase noise of 81 mrad recorded over 25 min. The amplifier is pumped by a ~1.1 ps, Yb-YAG, thin-disk regenerative amplifier and seeded with a supercontinuum generated in bulk YAG from the same pump pulses. Carrier-envelope phase stability is passively achieved through difference-frequency generation between pump and seed pulses. An additional active stabilization at 10 kHz combining 2f-to-f interferometry and a $LiNbO_3$ acousto-optic programmable dispersive filter achieves a record low phase noise.

OCIS codes: (320.7090) Ultrafast lasers; (190.4360) Nonlinear optics, devices; (190.4970) Parametric oscillators and amplifiers; (140.3070) Infrared and far-infrared lasers.

References and links

1. P. B. Corkum, "Plasma perspective on strong field multiphoton ionization," Phys. Rev. Lett. **71**(13), 1994–1997 (1993).
2. Ch. Spielmann, N. H. Burnett, S. Sartania, R. Koppitsch, M. Schnürer, C. Kan, M. Lenzner, P. Wobrauschek, and F. Krausz, "Generation of coherent X-rays in the water window using 5-femtosecond laser pulses," Science **278**(5338), 661–664 (1997).
3. E. J. Takahashi, T. Kanai, K. L. Ishikawa, Y. Nabekawa, and K. Midorikawa, "Coherent water window x ray by phase-matched high-order harmonic generation in neutral media," Phys. Rev. Lett. **101**(25), 253901 (2008).
4. T. Popmintchev, M.-C. Chen, D. Popmintchev, P. Arpin, S. Brown, S. Ališauskas, G. Andriukaitis, T. Balčiunas, O. D. Mücke, A. Pugzlys, A. Baltuška, B. Shim, S. E. Schrauth, A. Gaeta, C. Hernández-García, L. Plaja, A. Becker, A. Jaron-Becker, M. M. Murnane, and H. C. Kapteyn, "Bright coherent ultrahigh harmonics in the keV x-ray regime from mid-infrared femtosecond lasers," Science **336**(6086), 1287–1291 (2012).
5. M. Zürch, C. Kern, and C. Spielmann, "XUV coherent diffraction imaging in reflection geometry with low numerical aperture," Opt. Express **21**(18), 21131–21147 (2013).
6. H. Tomizawa, T. Sato, K. Ogawa, K. Togawa, T. Tanaka, T. Hara, M. Yabashi, H. Tanaka, T. Ishikawa, T. Togashi, S. Matsubara, Y. Okayasu, T. Watanabe, E. J. Takahashi, K. Midorikawa, M. Aoyama, K. Yamakawa, S. Owada, A. Iwasaki, and K. Yamanouchi, "Stabilization of a high-order harmonic generation seeded extreme ultraviolet free electron laser by time-synchronization control with electro-optic sampling," High Power Laser Sci. Eng. **3**, e14 (2015).
7. N. G. Johnson, O. Herrwerth, A. Wirth, S. De, I. Ben-Itzhak, M. Lezius, B. Bergues, M. F. Kling, A. Senftleben, C. D. Schröter, R. Moshammer, J. Ullrich, K. J. Betsch, R. R. Jones, A. M. Sayler, T. Rathje, K. Rühle, W. Müller, and G. G. Paulus, "Single-shot carrier-envelope-phase-tagged ion-momentum imaging of nonsequential double ionization of argon in intense 4-fs laser fields," Phys. Rev. A **83**(1), 013412 (2011).
8. A. D. Shiner, C. Trallero-Herrero, N. Kajumba, H.-C. Bandulet, D. Comtois, F. Légaré, M. Giguère, J.-C. Kieffer, P. B. Corkum, and D. M. Villeneuve, "Wavelength scaling of high harmonic generation efficiency," Phys. Rev. Lett. **103**(7), 073902 (2009).
9. B. M. Luther, K. M. Tracy, M. Gerrity, S. Brown, and A. T. Krummel, "2D IR spectroscopy at 100 kHz utilizing a Mid-IR OPCPA laser source," Opt. Express **24**(4), 4117–4127 (2016).
10. A. Thai, M. Hemmer, P. K. Bates, O. Chalus, and J. Biegert, "Sub-250-mrad, passively carrier-envelope-phase-stable mid-infrared OPCPA source at high repetition rate," Opt. Lett. **36**(19), 3918–3920 (2011).

#280369 http://dx.doi.org/10.1364/OE.25.001505
Journal © 2017 Received 11 Nov 2016; revised 13 Jan 2017; accepted 13 Jan 2017; published 19 Jan 2017

Optics EXPRESS

11. B. W. Mayer, C. R. Phillips, L. Gallmann, and U. Keller, "Mid-infrared pulse generation via achromatic quasi-phase-matched OPCPA," Opt. Express **22**(17), 20798–20808 (2014).
12. M. Baudisch, H. Pires, U. Elu, H. Ishizuki, T. Taira, and J. Biegert, "44 μJ, 160 kHz, few-cycle mid-IR OPCPA with chirp reversal," in Proceedings of CLEO OSA Technical Digest, paper STu3I.5 (2016).
13. B. W. Mayer, C. R. Phillips, L. Gallmann, M. M. Fejer, and U. Keller, "Sub-four-cycle laser pulses directly from a high-repetition-rate optical parametric chirped-pulse amplifier at 3.4 μm," Opt. Lett. **38**(21), 4265–4268 (2013).
14. M. Mero, F. Noack, F. Bach, V. Petrov, and M. J. J. Vrakking, "High-average-power, 50-fs parametric amplifier front-end at 1.55 μm," Opt. Express **23**(26), 33157–33163 (2015).
15. P. Rigaud, A. Van de Walle, M. Hanna, N. Forget, F. Guichard, Y. Zaouter, K. Guesmi, F. Druon, and P. Georges, "Supercontinuum-seeded few-cycle mid-infrared OPCPA system," Opt. Express **24**(23), 26494–26502 (2016).
16. H. Fattahi, H. G. Barros, M. Gorjan, T. Nubbemeyer, B. Alsaif, C. Y. Teisset, M. Schultze, S. Prinz, M. Haefner, M. Ueffing, A. Alismail, L. Vámos, A. Schwarz, O. Pronin, J. Brons, X. T. Geng, G. Arisholm, M. Ciappina, V. S. Yakovlev, D.-E. Kim, A. M. Azzeer, N. Karpowicz, D. Sutter, Z. Major, T. Metzger, and F. Krausz, "Third-generation femtosecond technology," Optica **1**(1), 45–63 (2014).
17. R. R. Alfano, *The supercontinuum laser source*, (Springer, 2016).
18. H. Fattahi, H. Wang, A. Alismail, G. Arisholm, V. Pervak, A. M. Azzeer, and F. Krausz, "Near-PHz-bandwidth, phase-stable continua generated from a Yb:YAG thin-disk amplifier," Opt. Express **24**(21), 24337–24346 (2016).
19. A. van de Walle, M. Hanna, F. Guichard, Y. Zaouter, A. Thai, N. Forget, and P. Georges, "Spectral and spatial full-bandwidth correlation analysis of bulk-generated supercontinuum in the mid-infrared," Opt. Lett. **40**(4), 673–676 (2015).
20. M. Bradler and E. Riedle, "Temporal and spectral correlations in bulk continua and improved use in transient spectroscopy," J. Opt. Soc. Am. B **31**(7), 1465–1475 (2014).
21. D. Majus and A. Dubietis, "Statistical properties of ultrafast supercontinuum generated by femtosecond Gaussian and Bessel beams: a comparative study," J. Opt. Soc. Am. B **30**(4), 994–999 (2013).
22. I. Gražulevičiūtė, M. Skeivytė, E. Keblytė, J. Galinis, G. Tamošauskas, and A. Dubietis, "Supercontinuum generation in YAG and sapphire with picosecond laser pulses," Lith. J. Phys. **55**(2), 110–116 (2015).
23. A.-L. Calendron, H. Çankaya, G. Cirmi, and F. X. Kärtner, "White-light generation with sub-ps pulses," Opt. Express **23**(11), 13866–13879 (2015).
24. A. Baltuska, M. Uiberacker, E. Goulielmakis, R. Kienberger, V. S. Yakovlev, T. Udem, T. W. Hansch, and F. Krausz, "Phase-controlled amplification of few-cycle laser pulses," IEEE J. Sel. Top. Quantum Electron. **9**(4), 972–989 (2003).
25. F. Lücking, V. Crozatier, N. Forget, A. Assion, and F. Krausz, "Approaching the limits of carrier-envelope phase stability in a millijoule-class amplifier," Opt. Lett. **39**(13), 3884–3887 (2014).
26. G. Gitzinger, V. Crozatier, R. Maksimenka, S. Grabielle, N. Forget, S. Alisauskas, A. Pugzlys, A. Baltuska, B. Monoszlai, C. Vicario, and C. P. Hauri, "Multi-octave acousto-optic spectrum analyzer for mid-infrared pulsed sources," in *CLEO: 2014*, paper STh1N.5, OSA Technical Digest (2014).
27. M. Baudisch, M. Hemmer, H. Pires, and J. Biegert, "Performance of MgO:PPLN, KTA, and $KNbO_3$ for mid-wave infrared broadband parametric amplification at high average power," Opt. Lett. **39**(20), 5802–5805 (2014).

1. Introduction

High-harmonic generation (HHG) [1] has become a routine technique to generate extreme-ultraviolet (XUV) radiation with full spatial and temporal coherence. The extension of HHG into the K-band water window (2.3 nm < λ < 4.4 nm) [2,3] and up to the keV photon energy regime [4] shows that fully coherent soft-x-ray beams/pulses could be produced from table-top ultrafast sources, promising probing and imaging [5] capabilities with unmatched tempo-spatial resolution. HHG sources have also been identified as potential seeders for free-electron lasers [6] to replace the current seeding schemes based on self-amplified spontaneous emission.

This extension towards XUV and up to soft-x-rays results from the recent development of driving sources with specific properties: mid-infrared wavelength, few-cycle pulses, high peak intensity, carrier-envelope phase stability and control, high energy and/or high-repetition rates. While long wavelength optical carriers extend the cutoff energy through the λ^2 dependency of the ponderomotive energy, shortening the pulses to few cycles increases the peak intensity and enhances the HHG conversion yield. Additionally, few-cycle pulses reduce the number of attosecond bursts up to, ideally, a single isolated attosecond pulse. In that case, CEP stability and control is paramount but also ensure a shot-to-shot reproducibility of the driving electric field as well as the HHG yield and spectra (especially for few-cycle pulses).

Optics EXPRESS

Besides, although phase-tagging [7] may be used for data post-processing, precise stabilization offers the unparalleled advantage of direct data averaging and/or heterodyning. Last, high pulse energy and/or repetition rate helps mitigating the λ^{-6}-λ^{-7} scaling law of the HHG yield [8] for an optimized XUV flux.

These requirements have triggered the development of a number of high-repetition-rate sources [9–15] combining nonlinear effects such as difference-frequency generation (DFG) and optical parametric amplification (OPA) to, respectively, generate and amplify broadband mid-infrared pulses within the 3-5 μm range. In both cases, energy is transferred, via local and instantaneous three-wave-mixing process, from a "pump" wave of angular frequency ω_p to a "signal" wave of angular frequency $\omega_s < \omega_p$. An "idler" wave at ω_i is generated as a by-product of parametric amplification to satisfy the energy conservation relationship $\hbar\omega_p = \hbar\omega_s + \hbar\omega_i$. For efficient operation when phase-matching conditions are fulfilled (momentum conservation), the phases of the three waves also satisfy φ_p-φ_s-$\varphi_i = \pi/2$. Finally, the Manley-Rowe relationship binds together the photon fluxes of the three waves and limits the maximum conversion yield from pump to signal wave to ω_s/ω_p. Therefore, it is clearly advantageous to pump OPAs with a pump wavelength as close as possible to the signal wavelength. The recent advent of scalable, picosecond, high-average-power infrared sources based on Yb:YAG has set these laser sources as the main work horses for broadband OPAs which are now described as "third-generation femtosecond technology" [16].

Previously demonstrated mid-IR DFG/OPA systems [9–15] differ in the characteristics of the pump laser (wavelength and pulse duration) but mostly in the way the signal and pump pulses are synchronized. Systems pumped by multi-ps (1-10 ps), 0.1-1 mJ pulses at repetition rates greater than 100 kHz are seeded by either optical parametric oscillators [9], or erbium-doped fiber-based femtosecond sources [10,11]. Although these solutions all lead to the generation of large optical spectra around either 1550 nm or 3 μm, they involve rather complex setups requiring active electronic locking of independent laser systems [9], or additional nonlinear effects to derive the pump seed from a signal oscillator [9–11]. In the latter case, the amplification process of the pump pulses introduces long optical delay which necessitates complex active stabilization to reduce delay jitter and drift between pump and signal pulses.

An alternative, which greatly simplifies the global architecture and provides robust passive optical synchronization between pump and seed pulses, is to use a small fraction of the pump laser energy to generate a supercontinuum (SC) via filamentation in a bulk material [17]. It is now well-known that, within the single-filament limit, the high- and low- frequency parts of a SC provide broadband, coherent [18] and stable [19–21] spectral content, even when driven by ~1 ps pulses at ~1 μm [22,23]. Additionally, the properties of the carrier-envelope phase of the SC essentially follow that of the pump pulse, a stupendous feature at the very heart of f-2f interferometry [24] and of the passive CEP-stabilization of idler pulses generated in self-seeded OPAs through a DFG process.

In this paper, we demonstrate and study a supercontinuum-seeded optical chirped-pulse parametric amplifier (OPCPA) generating few cycle pulses around 3.1 μm and optimized for CEP-stability. This source delivers 40-μJ, 40-fs pulses at 100 kHz repetition rate, which corresponds to a peak power of ~0.4 GW, an average power of 4 W and a pulse duration slightly under four optical cycles. Compared to former publications, and in particular to references [11,15], our source provides important novel features:

(i) It is the first 100-kHz-class OPCPA pumped with a diode-pumped solid-state laser delivering 1-ps pulses and self-seeded with an infrared supercontinuum generated in a bulk crystal,

(ii) Combines chirp-reversal with acousto-optic pulse shaping at 100 kHz and delivers, to date, the shortest pulses at this wavelength (3.1 μm) and average power (4W),

Optics EXPRESS

(iii) Achieves a non-averaged CEP stability with a phase noise as low as 81 mrad rms over more than $150 \cdot 10^6$ pulses (25 min at 100 kHz). To date this is the best recorded non-averaged CEP stability for an amplified system, independently of the wavelength, pulse duration or repetition rate [25].

2. Source description

The OPCPA is pumped by a fraction of an industrial Yb-YAG, thin-disk, regenerative amplifier (Dira-200 from TRUMPF Scientific Lasers) generating 2-mJ pulses at 1030 nm at the repetition rate of 100 kHz (average power of 200 W). The pulse duration at full-width half-maximum (FWHM) is 1.1 ps. The beam profile is close to Gaussian (measured $M^2<1.3$) and the typical pulse-to-pulse energy stability is <1% rms. About 55 W of pump power is used to pump the OPCPA in its current configuration (Fig. 1). The remaining 145 W is saved for a future upgrade of the system.

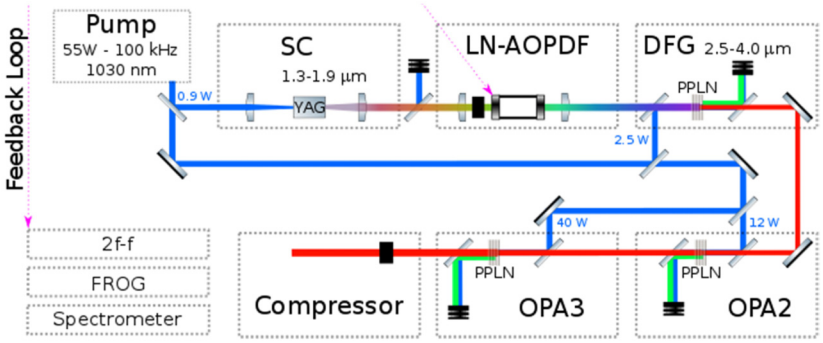

Fig. 1. Optical setup. SC: supercontinuum generation. DFG: difference-frequency generation. OPA: optical parametric amplifier. LN-AOPDF: $LiNbO_3$ acousto-optic programmable dispersive filter.

A small fraction (9 µJ) of the pump energy is used to generate a supercontinuum in a 10-mm YAG crystal mounted on a continuously moving translation stage. The crystal is translated transversally along a single direction, over 3 mm with a period of 10 min. A stable single-filament is formed in the bulk of the crystal and maintained for months without any visible permanent damage. A noticeable temperature elevation of the crystal is observed and stabilized around 10°C above ambient temperature by passive cooling. Filament instabilities and spectral modulation are noted above 12 µJ pump energy and immediate damage is observed for pump energies exceeding 14 µJ. These observations are in agreement with the previously reported data for both the SC threshold and nonlinear absorption of YAG [22,23]. At the output of the filament, the SC spectrum extends to ~2 µm (Fig. 2).

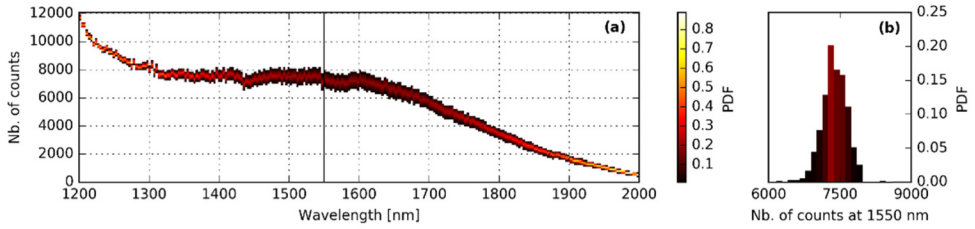

Fig. 2. (a) Supercontinuum spectra (red part) recorded by an InGaAs spectrometer (NIRQuest-2.5, Ocean Optics) with an integration time of 1 ms. Shown here is the probability density function (PDF) computed from 1000 successive acquisitions. (b) Cut at 1550 nm of the PDF showing a histogram with 5.7% rms.

Optics EXPRESS

The infrared part of the SC is filtered and temporally stretched by an AR-coated, 18-mm-long Silicon rod and a Lithium Niobate ($LiNbO_3$) acousto-optic programmable dispersive filter (LN-AOPDF, Fastlite), specifically developed for this application. Compared to TeO_2-based AOPDFs, LN-AOPDFs are capable of refresh rates exceeding 100 kHz and have large angular acceptance (~6°) and ultra-low spatial walk-off. This device is at the heart of the spectral/dispersion management and performs: phase shaping of the SC pulses to match the pump pulse duration; bandwidth selection and amplitude shaping of the SC spectrum; pre-compensation of the high-order spectral phase introduced by the optics; and last but not least, active CEP stabilization with a feedback from a 2f-to-f interferometer.

Shaped seed pulses are focused in a 12x3x1-mm^3 MgO-doped periodically poled Lithium Niobate crystal (MgO-PPLN) AR-coated at 1030 nm and from 1.3 to 4.2 µm. The crystal is heated to 120°C to limit photorefractive effects. The poling period varies across the 12-mm direction (so-called "fanout" poling geometry) to fulfill type-0 quasi-phase-matching conditions from 1.3 µm to 1.9 µm (for the signal) and 2.5 µm to 4.0 µm (for the idler). The MgO-PPLN of the DFG stage is pumped with 2.5 W (25 µJ) at 1030 nm and the calculated peak intensity is ~50 GW/cm^2 (3D Gaussian). Pump, signal and/or idler beams are combined and separated before and after the MgO-PPLN by pairs of dichroic mirrors. The spectrum of CEP-stable idler pulses produced by DFG is optimally centered at 3.1 µm and extends from 2.7 µm to 3.6 µm. The FWHM spectral bandwidth is 0.44 µm and the pulse energy is 0.9 µJ.

The generated mid-infrared pulses are successively amplified in two travelling-wave OPA stages (OPA2 and OPA3 on Fig. 1). Both stages use MgO-PPLN crystals as nonlinear medium and crystals are identical to the one of the DFG stage but for the thickness of the poled area: 0.5 mm for OPA2 and 0.7 mm for OPA3, instead of 1 mm for DFG. The pump power (and calculated peak intensity) in OPA2 and OPA3 is respectively 12.5 W (~35 GW/cm^2) and 40 W (~25 GW/cm^2). The output power at 3.1 µm, measured behind the dichroic mirrors, is respectively 0.8 W and 4 W. The output spectrum is measured by a scanning acousto-optic spectrum analyzer (Mozza, Fastlite) [26]. Figure 3(a) shows the output spectra after DFG (FWHM = 503 nm, 4σ = 706 nm), OPA2 (FWHM = 455 nm, 4σ = 681 nm) and OPA3 (FWHM = 480 nm, 4σ = 651 nm). The conversion efficiency, calculated as $(P_{s,out} - P_{s,in} + P_{i,out})/P_{p,in}$ where $P_{s,in}$, $P_{s,out}$,$P_{i,out}$,$P_{p,in}$ are the average powers of, respectively, output signal, input signal, output idler and input pump beams is ~17% for OPA2 and ~24% for OPA3. This calculation does not take into account the optical losses on the faces of the MgO-PPLN crystals, the losses on the dichroic mirrors (4 interfaces) and the parasitic effects in the nonlinear crystals (non-phase-matched SHG at the pump wavelength for example). The pump-to-idler conversion efficiency thus reads 6.4% for OPA2 and 10% for OPA3. The overall efficiency to generate 3.1 µm is 4W/55W = 7.2%.

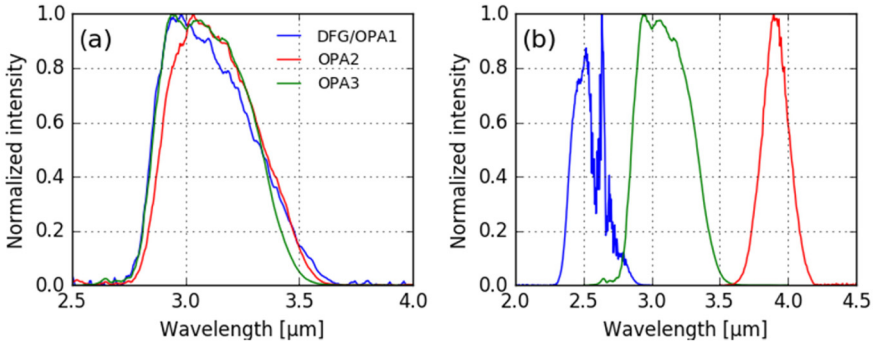

Fig. 3. (a) Spectra after DFG (blue), OPA2 (red) and OPA3 (green). (b) Output spectra at 2.5 µm (blue), 3.1 µm (green) and 3.9 µm (red) obtained by adjusting AOPDF settings, delays and PPLN period of the different stages.

Optics EXPRESS

The output beam is expanded by a reflective telescope and compressed in a set of AR-coated silicon flats corresponding to a total thickness of 14 mm.

3. Dispersion management and tunability

Durations of pump and signal pulses are simultaneously matched in all OPAs by means of the AOPDF and by combining materials having positive (Silicon) and negative (CaF_2) group velocity dispersions (GVD) in the 2.5-4 µm range. The thicknesses of the optics (dichroic mirrors, lenses…) were selected to achieve a near perfect GVD balance at 3 µm between the DFG and OPA2 stages but also the OPA2 and OPA3 stages. When the wavelength is tuned, this balance is partly lost and the pump-signal duration match cannot be perfectly maintained in all OPAs simultaneously (without adding CaF_2 or Silicon windows, which was not done here). Indeed, once the AOPDF is set to match the pulse duration in OPA3, there is no additional available degree of freedom to control the durations of the seed pulse in the DFG and OPA2 stages. This duration mismatch results in spectral narrowing or a reduced conversion efficiency depending on the seed duration which respect to that of the pump pulse.

The OPCPA output spectrum can be tuned by translating the MgO-PPLN crystals transversally and by adjusting the settings of the AOPDF and the delay lines. Tunability from ~2.5 µm to ~3.9 µm (central wavelength) has been demonstrated. Figure 3(b) shows the spectra obtained for three different settings and for the same pump power. The output powers at 2.5 µm, 3.1 µm and 3.9 µm are 1.5 W, 4W and 0.5 W respectively. The spectral structures on the spectrum centered at ~2.5 µm result from absorption in ambient water vapor. Since the gain bandwidth for type-0 phase-matching is maximum close to degeneracy at 2.06 µm, broader spectra could have been expected at around 2.5 µm. The observed result can be explained by the lower seed level available at 1.75 µm for the DFG, and also, as explained above, by a mismatch between the durations of the pump and signal pulses.

4. Output energy stability

An average output power of ~4W was measured by a powermeter (UP25N-40S, Gentec) over 25 min.

In order to monitor the pulse-to-pulse stability of the pump, SC and output pulses, fractions of these beams are sampled out and sent to amplified photodiodes: InGaAs photodiode for the pump pulses, extended-InGaAs photodiode for the SC pulses, HgCdTe photodiode for the output pulses. The output signals are simultaneously recorded at 100 kHz (synchronous acquisition) and the resulting data are stored and processed. For 100 successive shots, recorded data show an output pulse-to-pulse energy variations of ~1.3% rms, while the energy variations of the pump pulses are ~0.9% rms. Remarkably, the energy stability improves from DFG (~4.7% rms) to OPA3 (~1.3% rms) indicating the increasing level of saturation within the successive nonlinear stages. In order to demonstrate long-term pulse energy trends (power drift), the data averaged over $2 \cdot 10^5$ pulses at each point are presented on Fig. 4.

Optics EXPRESS

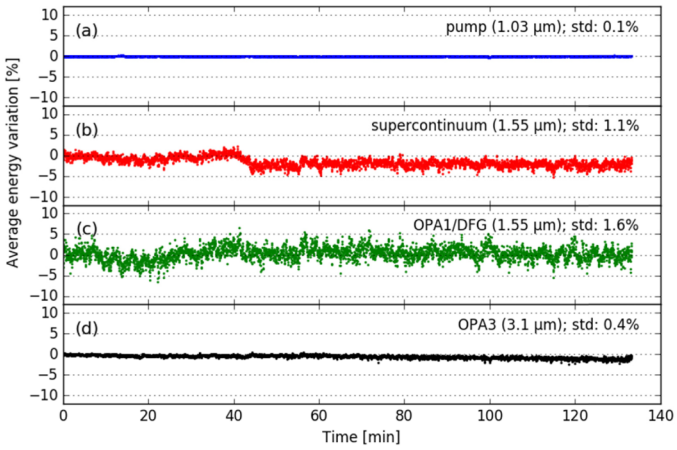

Fig. 4. Average energy variation as a function of time. Each point is an average over 2 sec ($2 \cdot 10^5$ shots). (a) pump (0.1% rms), (b) supercontinuum after a high-pass filter with a cut-off at 1.3 μm (~1.1% rms), (c) DFG (amplified seed, ~1.6%) and (d) output (OPA3) (~0.4% rms).

As in [11,15,27], we report the onset of nonlinear and/or thermal effects limiting the output power of the OPAs and, in particular, of OPA3, where the pump and idler powers are the highest. The parameters of the last OPA stage are intermediate between those given in [15] and in [27] and essentially differ by: the thickness of the MgO-PPLN crystals (with respect to [26]), the pump pulse duration (with respect to [15,27]) and the contrast of the pump pulses (with respect to [27]). Although deeper investigation would be required, our results tend to confirm that these effects originate from combined mid-IR-assisted nonlinear absorption and thermal effects.

5. Beam characterization

The spatial beam profile was characterized by a scanning slit beam profiler (NanoScan, Ophir Photonics) integrating a pyroelectric detector and a slit of 5 μm. The spatial profile, measured after a ~50 cm free propagation after OPA3 and before the output telescope, is Gaussian-like, with a ~2.2 mm beam diameter at FWHM (Fig. 5). After collimation by a pair of concave mirrors, the beam was focused by an f = 500 mm lens and the 4σ beam diameter was measured as a function of distance from the waist. Following the method described in ISO-11146, we measured a $M^2 = \sqrt{M_X^2 M_Y^2}$ value <1.3.

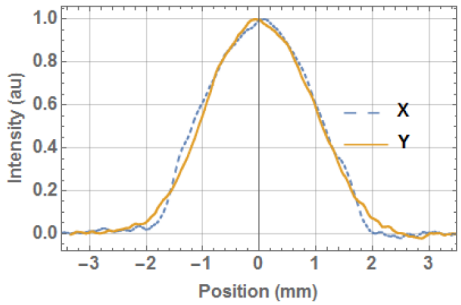

Fig. 5. Near-field spatial profiles along horizontal (X) and vertical (Y) directions

6. Pulse characterization

Fractions of the output beam are sent to a scanning SH-FROG device to characterize the pulse duration and spectral phase and to a 2f-to-f interferometer to monitor the CEP drift. The SH-

Optics EXPRESS

FROG was built from a thin broadband KBr beamsplitter with a reflectivity of 50 ± 5% over the full 2-5 µm bandwidth, a 100-µm silver thiogallate (AgGaS2) crystal oriented for type-I second harmonic generation, and an InGaAs spectrometer (NIRQuest-2.5, OceanOptics). The experimental and reconstructed FROG traces are shown on Fig. 6. The retrieved pulse duration (<0.4% rms error over a 160x160 calculation grid) is 38.3 ± 1 fs at FWHM, which is within 8% of the Fourier-transform limit (35.7 ± 1 fs). The uncertainty on the latter values arises from the limited dynamic range of the FROG measurement and the inevitable choice of a spectral threshold to distinguish signal from background and noise. The spectral barycenter being at 3.1 µm, such a pulse duration corresponds to less than 4 optical cycles (an optical cycle is 10.3 fs at 3.1 µm).

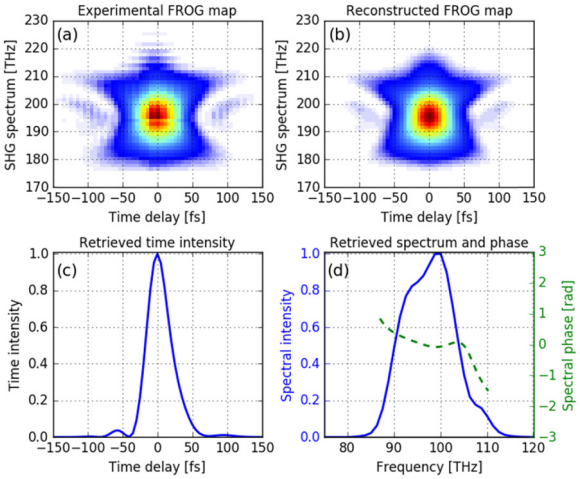

Fig. 6. (a) Experimental FROG trace. (b) Retrieved FROG trace. (c) Reconstructed time-dependent intensity. (d) Reconstructed spectrum and spectral phase.

The stability and drift of the CEP was assessed by nonlinear interferometry. However, unlike previous works, and in particular [24] and [10] which are respectively based on f-to-2f and 2f-to-3f interferometry, we use a 2f-to-f scheme in which the SHG occurs before the spectral broadening step, and all statistical values are calculated from single-shot acquisitions (i.e. not averaged over a large number of shots): the collimated input beam (~10 µJ) first propagates through a thin type-I SHG crystal ($AgGaS_2$) and is then focused in a 4-mm YAG crystal to generate a stable continuum extending to the visible. The spectral beating around 1.55 µm, which arises from the interference between the second harmonic of the input pulse and the continuum, is recorded by a fast spectrometer with onboard calculation capabilities ([25], Fringeezz, Fastlite). In this 2f-to-f scheme, the optical delay between the two components at 1.55 µm is directly related to the thickness of the YAG crystal, which allows a straightforward optimization of this delay in order to match the spectral resolution of the spectrometer. The latter device consists of a slit, a high-efficiency transmission grating, a pair of AR-coated lenses and an InGaAs linear array with a minimum integration time of 3 µs. All components are selected to minimize the optical losses and maximize the signal-to-noise ratio on the detector. As a result, the detector could be saturated even at the minimal integration time (i.e. for single-shot acquisition). The analog beating signal is recorded and the phase drift of the interferogram is computed and stored at 10 kHz. With this setup, the CEP drift between isolated pulses is sub-sampled at 10 kHz (single-shot every ten pulses). As a result, noise contributions above 5 kHz are aliased.

A digital output is used to feed back at 10 kHz the CEP drift to the AOPDF and correct for the CEP fluctuations. The feedback loop is a simple proportional correction with a damping factor of 0.5 (damping factor was limited to $1/2^N$ values by the hardware), time-

Optics EXPRESS

delayed with a latency time of ~60 µs, meaning that the phase correction applied to the pulses from N + 6 to N + 16 is 50% of the phase shift measured for the pulses N-10 to N.

An example of CEP fluctuations over ~80 s without feedback is shown on Figs. 7(a) and 7(b). As the number of acquired values exceeds 800 000 points, Fig. 7(a) represents the probability density function (PDF) as a function of time rather than the values directly. On Fig. 7(b), the distribution of the values is mostly Gaussian with a standard deviation of 255 mrad.

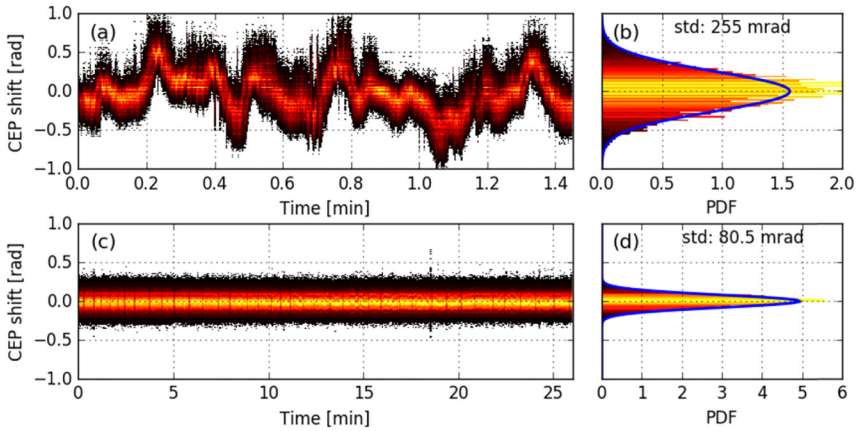

Fig. 7. (a) open-loop CEP noise PDF as a function of time, (b) open-loop CEP noise histogram, the standard deviation is 255 mrad, the blue curve is a Gaussian function with a σ parameter corresponding to the histogram standard deviation, (c) close-loop CEP noise PDF as a function of time, (d) close-loop CEP noise histogram, the standard deviation is 80.5 mrad, the blue curve is a Gaussian function with a σ parameter corresponding to the histogram standard deviation. Colors from dark to bright denote the probability density from low to high, respectively.

In closed-loop operation (Figs. 7(c) and 7(d)), the CEP in-loop fluctuations are below 81 mrad rms with a peak-to-peak variation below 1 rad over 25 min, which corresponds to $15 \cdot 10^6$ samples at 10 kHz or $150 \cdot 10^6$ successive pulses (i.e. equivalent to ~42 h at 1 kHz). h at 1 kHz) Fig. 8(a) shows the comparison of the power spectral densities in open- and closed-loop operations. This figure and Fig. 8(b), representing the integrated phase noise, show a complete noise canceling at all contributing frequencies below ~1 kHz and a residual noise in the 2-5 kHz range, which is in accord with the Nyquist frequency of the measurement device (5 kHz) and the damping factor (0.5) used for the feedback. Further analysis of the noise content requires a better understanding of the resolution of the detector and signal-to-noise ratio of the InGaAs linear array (estimated to be ~100), but also of the intensity-to-CEP coupling effects in the continuum generation [24].

Optics EXPRESS

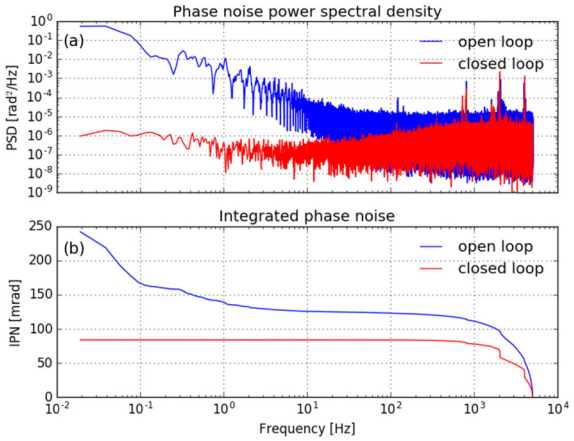

Fig. 8. (a) Phase noise power spectral densities for open and closed loops, (b) integrated phase noise (IPN) for open and closed loops.

7. Conclusion and prospects

The OPCPA system presented here shows an excellent long term power stability with power fluctuations of 0.4% rms over 2 hours, thanks to its collinear geometry, self-seeded design and all-bulk dispersion management. The mid-IR wavelength, centered at 3.1 µm, coupled to <4-cycle pulse duration and pulse energy of 40 µJ, should allow for the HHG in the soft-x-ray regime. From the measured data, a peak intensity of $>10^{14}$ W/cm^2 is at reach with a focal spot of 25 µm FWHM. The long-wavelength operation and a record low CEP fluctuations of 81 mrad rms, combined with a proper post-compression setup, would also form an ideal tool to generate isolated attosecond pulses in the water window.

With the addition of another OPA stage, pumped with the remaining 145 W of pump power, an output pulse energy of 150 µJ is targeted, which would raise the output average power from 4 W to 15 W and pave the route to high flux HHG sources in the water window.

Funding

ELI-HU Non-Profit Ltd and the European Union's Horizon 2020 research and innovation program under the Marie Sklodowska Curie grant agreement No. 641; Fond unique interministériel (FUI AAP17 – projet STAR).

Acknowledgments

The publication reflects only the author's view. The Research agency of the European Union is not responsible for any use that may be made of the information it contains. We also acknowledge the early-stage participation and subsequent fruitful discussions with Alexandre Thai.